ISSN 1063-7834, Physics of the Solid State, 2020, Vol. 62, No. 7, pp. 1136–1144. © Pleiades Publishing, Ltd., 2020.
Russian Text © The Author(s), 2020, published in Fizika Tverdogo Tela, 2020, Vol. 62, No. 7, pp. 1008–1016.

SUPERCONDUCTIVITY

Model of the Behavior of a Granular HTS in an External Magnetic Field: Temperature Evolution of the Magnetoresistance Hysteresis

S. V. Semenov[a, b, *] and D. A. Balaev[a, b]

[a] *Kirensky Institute of Physics, Krasnoyarsk Scientific Center, Siberian Branch, Russian Academy of Sciences, Krasnoyarsk, 660036 Russia*

[b] *Siberian Federal University, Krasnoyarsk, 660041 Russia*

**e-mail: svsemenov@iph.krasn.ru*

Received February 13, 2020; revised February 13, 2020; accepted February 18, 2020

Abstract—A model for describing the magnetoresistance behavior in a granular high-temperature superconductor (HTS) that has been developed in the last decade explains a fairly extraordinary form of the hysteretic $R(H)$ dependences at T = const and their hysteretic features, including the local maximum, the negative magnetoresistance region, and the local minimum. In the framework of this model, the effective field $\mathbf{B}_{\text{eff}}$ in the intergrain medium has been considered, which represents a superposition of the external field and the field induced by the magnetic moments of HTS grains. This field can be written in the form $\mathbf{B}_{\text{eff}}(H) = \mathbf{H} + 4\pi\alpha\mathbf{M}(H)$, where $M(H)$ is the experimental field dependence of the magnetization and α is the parameter of crowding of the magnetic induction lines in the intergrain medium. Therefore, the magnetoresistance is a function of not simply an external field, but also the "internal" effective field $R(H) = f(\mathbf{B}_{\text{eff}}(H))$. The magnetoresistance of the granular $YBa_2Cu_3O_{7-\delta}$ HTS has been investigated in a wide temperature range. The experimental hysteretic $R(H)$ dependences obtained in the high -temperature range (77–90 K) are well explained using the developed model and the parameter α is 20–25. However, at a temperature of 4.2 K, no local extrema are observed, although the expression for $\mathbf{B}_{\text{eff}}(H)$ predicts them and the parameter α somewhat increases (~30–35) at this temperature. An additional factor that must be taken into account in this model can be the redistribution of the microscopic current trajectories, which also affects the dissipation in the intergrain medium. At low temperatures under the strong magnetic flux compression (α ~ 30–35), the microscopic trajectories of the current $\mathbf{I}_m$ can change and tunneling through the neighboring grain is preferred, but the angle between $\mathbf{I}_m$ and $\mathbf{B}_{\text{eff}}$ will be noticeably smaller than 90°, although the external (and effective) field direction is perpendicular to the macroscopic current direction.

Keywords: granular HTS, magnetoresistance hysteresis, grain boundaries

DOI: 10.1134/S1063783420070239

1. INTRODUCTION

Polycrystalline (hereinafter referred to as granular) high-temperature superconductors (HTSs) are two-level superconducting systems. These are superconducting crystallites with a strong superconducting subsystem that are coupled by the Josephson effect through grain boundaries, which form the second (weak) superconducting subsystem. The contribution of grain boundaries to the magnetic properties is only manifested in fairly weak magnetic fields (tens of oersted at low temperatures [1, 2] and fractions of oersted at high temperatures [2, 3]). In moderate and strong magnetic fields, the magnetization of granular HTSs is only determined by the grain response [4, 5] or, in fact, by the intragrain critical current [5, 6]. The subsystem of grain boundaries determines, in turn, the transport properties of granular HTSs, since superconducting current transport through a bulk sample occurs via carrier tunneling through the grain boundaries [7–9].

However, there is an interaction between these subsystems. It manifests itself, to the greatest extent, in the magnetotransport properties, i.e., the magnetic field dependences of the critical current [10–15] and magnetoresistance $R(H)$ [13–16]. For example, the $R(H)$ dependences exhibit a complex nonmonotonic hysteretic behavior [17–20], which was not explained in earlier works. Therefore, the model of the behavior of a granular HTS in an external magnetic field began to be formed only in the beginning of the century [21–44], when the studies devoted to detailed investigations of the magnetotransport properties occurred.

Briefly, the interaction between subsystems of grains and grain boundaries can be explained as follows. The magnetic induction lines from the magnetic

moments $\mathbf{M}_G$ of HTS grains are closed through the intergrain space (Fig. 1a). As a result, the field in the intergrain spacings differs from the external field and it is this field that affects tunneling between grains. The field $\mathbf{B}_{ind}$ induced by the magnetic moments $\mathbf{M}_G$ is proportional to the specific magnetization M (in fact, to the averaged magnetic moment of grains) and it will be a hysteretic function of the external field H due to the $M(H)$ hysteresis well-known for type-II superconductors. Therefore, the effective field $\mathbf{B}_{eff}$ in the intergrain medium can be written in the form

$$\mathbf{B}_{eff}(H) \sim \mathbf{H} + \mathbf{B}_{ind}(H). \quad (1)$$

Equation (1) explains the hysteretic nature of the $R(H)$ dependences, since the dissipation in the intergrain boundaries is determined by the effective field B_{eff}. The situation, however, is complicated by the effect of the magnetic flux compression. The fact is that the length of the intergrain boundaries is comparable with the superconducting coherence length (several nanometers), while the grain sizes are enormously larger (several or tens of microns). Such a difference in the sizes inevitably leads to the strong compression of the magnetic induction lines in the intergrain medium (see a schematic in Fig. 1b). The possible flux compression in the intergrain medium was first mentioned in [21]; later on, this was confirmed in experiments [45–51]. In particular, it was proposed to introduce a coefficient of proportionality between B_{ind} and magnetization M: $B_{ind} = 4\pi\alpha M$. Here, the parameter α characterizes the averaged effect of crowding the lines of magnetic induction B_{ind}. Then, Eq. (1) can be rewritten in the form

$$B_{eff}(H) = |H - 4\pi\alpha M(H)|. \quad (2)$$

Equation (2) takes into account the direction of the lines of magnetic induction B_{ind} relative to the external field H (Figs. 1a, 1b). The absolute value is taken because the resistance is an even function of the magnetic field (the factor 4π corresponds to the GHS system).

The magnetoresistance $R(H)$ of a granular superconductor is a function of B_{eff}. If we consider the dissipation processes using the standard approaches, for example, the Arrhenius relation $R(H) = R_{NJ}\exp(-U/kT)$, then it is necessary to understand that the Josephson coupling energy U (the equivalent of the Abrikosov vortex pinning potential for HTS grains) is, first of all, a function of the effective field, rather than the external field ($U(H) \to U(B_{eff})$). The described approach reproduces well the main features of the observed $R(H)$ dependences using Eq. (2) and experimental magnetization hysteresis loops $M(H)$ [52]. A detailed comparison of the hysteretic $R(H)$ dependences with the $B_{eff}(H)$ dependences showed that the parameter α of the 1–2–3 HTS structure is about 20–25 and the degree of compression almost does not change in the range from 77 K to the superconducting transition temperature (≈90 K) [50]. To further develop the model of the behavior of a granular HTS in an external magnetic field, the investigated

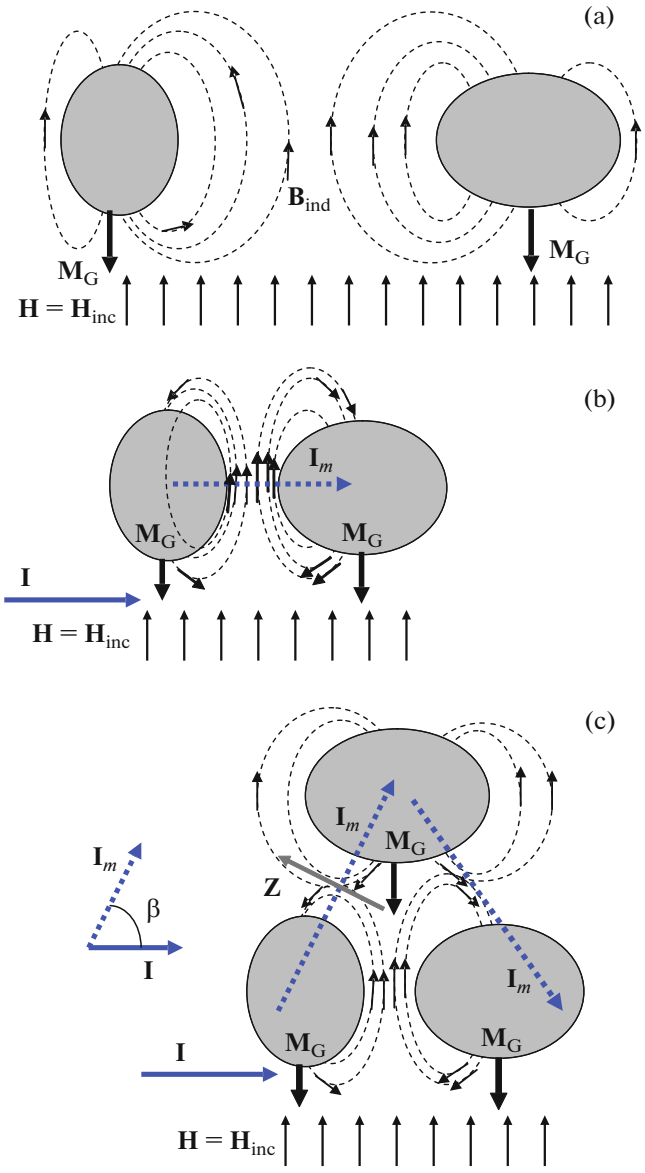

Fig. 1. Schematic of magnetic induction lines in the intergrain medium of a granular HTS. Ovals show HTS grains; the space between them is an intergrain medium; the intergrain spacings are significantly enlarged. Dashed lines show the lines of magnetic induction $\mathbf{B}_{ind}$ from the magnetic moments $\mathbf{M}_G$ of superconducting grains and arrows show the $\mathbf{B}_{ind}$ direction with an increasing external field $\mathbf{H} = \mathbf{H}_{inc}$. (a, b) Comparison of the cases of grains located far from and close to each other. In (b), the effect of crowding of the magnetic induction lines is implemented. In (b, c), $\mathbf{I}_m$ are the microscopic current trajectories, $\mathbf{I}$ is the macroscopic current direction at the perpendicular orientation $\mathbf{H} \perp \mathbf{I}$. In (c), the possible redistribution of the $\mathbf{I}_m$ trajectories is shown for a small angle between $\mathbf{I}_m$ and $\mathbf{B}_{ind}$ (see Section 3).

temperature range should be extended more significantly. In this work, we measured the hysteretic $R(H)$ dependences for the $YBa_2Cu_3O_7$ granular HTS sample both in the high-temperature region and at the liquid helium temperature. The main aim of this study was to follow the change in the shape of the $R(H)$ dependence with temperature to check, add, and further develop the model of a granular HTS.

2. EXPERIMENTAL

The $YBa_2Cu_3O_{7-\delta}$ HTS sample was fabricated by a standard solid-phase synthesis method from the corresponding oxides with three intermediate grindings. The final annealing was performed at a temperature of about 940°C close to the melting point for 50 h. After completion of the synthesis, the sample was annealed at a temperature of 350°C for 10 h to obtain the oxygen stoichiometry.

According to the X-ray diffraction data, all the reflections of the synthesized sample correspond to a 1-2-3 HTS; no foreign phases were detected. According to the scanning electron microscopy data obtained on a Hitachi-TM 3000 electron microscope, the average grain size d is ~10 μm and there are areas of coalescence of crystallites. The energy dispersive spectrometry study showed that the element ratio corresponds to the chemical formula $YBa_2Cu_3O_{7-\delta}$. The superconducting transition temperature T_c determined by the magnetic measurements (Fig. 2) was found to be 92.4 K.

The transport properties were measured by a standard four-probe method. The critical current density J_c was 150 A/cm^2 at a temperature of $T = 77$ K and 1.5 kA/cm^2 at $T = 4.2$ K (in zero external field). For the samples with these sufficiently high J_c values, the transport measurements face an experimental problem. The measurements should be performed at the transport current I comparable with the critical current I_c. If $I < I_c$ in some field H, then we have $R(H) = 0$; therefore, to measure the $R(H)$ dependences, it is necessary to meet the condition $I > I_c(H)$. For typical sample sizes of about $0.8 \times 0.8 \times 8$ mm^3 (the transport current I is applied along the long direction), at $T = 4.2$ K, the transport current I should be higher than ~200 mA and, to ensure the efficient removal of the heat released at the contacts, the sample should be placed in a cryogenic liquid. In this work, gold-plated pressed electrical contacts were used, which made it possible to avoid sample heating due to the heat generation on the current contacts at transport currents of up to 30 mA when a sample was in the helium heat-exchange atmosphere and up to at least 500 mA when a sample was placed directly in a cryogenic liquid. An external field set by either an electromagnet (high temperatures, $I = 30$ mA) or a superconducting solenoid was applied perpendicular to the transport current direction (**H** ⊥ **I**). The $R(H)$ measurements at the weak

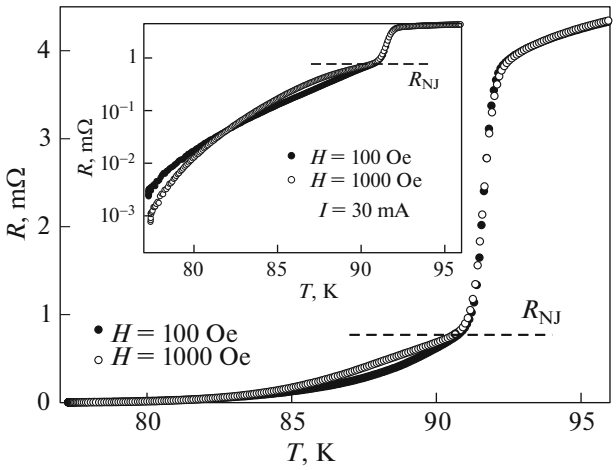

Fig. 2. Temperature dependences of the electrical resistance $R(T)$ for the investigated sample in external magnetic fields of 100 Oe and 1 kOe. Inset: the same in the semi-logarithmic coordinates. The horizontal dashed line corresponds to the total resistance R_{NJ} of the subsystem of grain boundaries.

($I = 1$ mA) transport current was performed on a PPMS-6000 facility. The magnetoresistance data obtained at high temperatures and at 4.2 K (in a cryostat with liquid helium) were obtained on the same sample.

The magnetic properties were studied on a vibrating sample magnetometer [53] under the external conditions corresponding to the magnetotransport measurements on the sample that was used to record the $R(H)$ dependences.

3. RESULTS AND DISCUSSION

Figure 2 shows temperature dependences of the electrical resistance $R(T)$ in external magnetic fields of 100 Oe and 1 kOe. The sharp resistance jump starting at $T_c \approx 92.4$ K and weakly depending on the external field corresponds to a transition in the subsystem of superconducting grains and the smooth portion of the $R(T)$ dependences reflects a transition of the subsystem of grain boundaries to the superconducting state [7, 15, 19, 20, 31, 32, 39]. Such a clear separation of the dissipation in the subsystems of grains and grain boundaries confirms the correctness of consideration of a granular HTS as a two-level subsystem (see Section 1). If we arbitrarily separate the total resistance of the sample as a sum of the resistances of grains and grain boundaries, then the R value near the beginning of the transition of grain boundaries can be considered to be the normal resistance R_{NJ} of this subsystem [54] (see Fig. 2).

For type-II superconductors, the $R(T)$ dependences in an external field are, as a rule, monotonic and, at $T = \text{const}$, the resistance increases with the

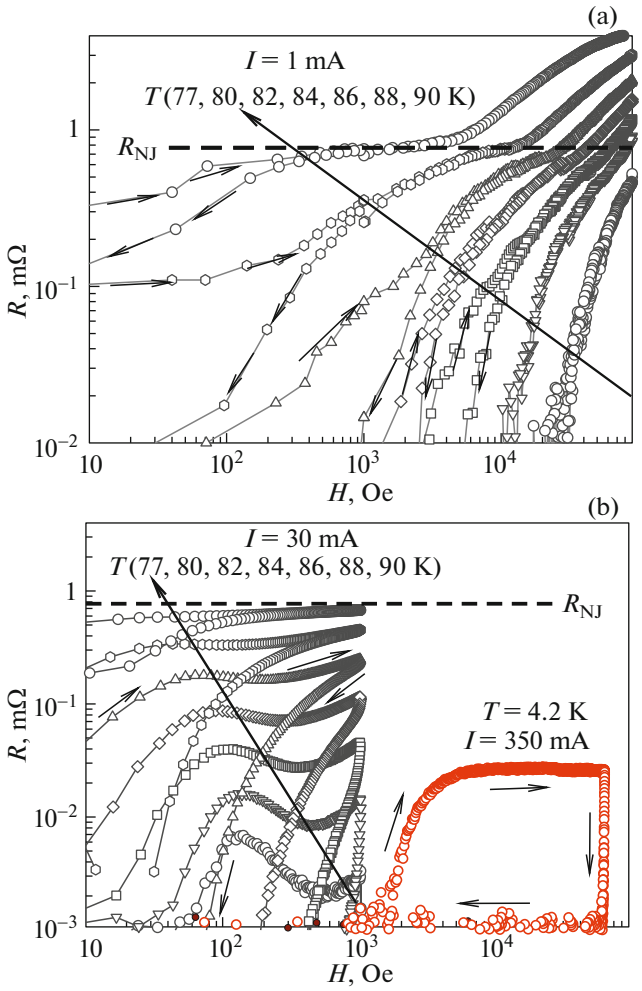

Fig. 3. Hysteretic $R(H)$ dependences at the indicated temperatures and transport currents I in a double logarithmic scale. Arrows show the external field variation direction. The R_{NJ} value (see Fig. 2) is shown by a horizontal dashed line.

external field [55]. A slightly different situation is illustrated in Fig. 1. The inset in Fig. 1 shows that the $R(T)$ dependences in external fields of 100 Oe and 1 kOe intersect and, in the temperature range of 77—82 K, we have $R(H = 1\ \text{kOe}) < R(H = 100\ \text{Oe})$, while at $T > 83$ K, a standard behavior is observed: $R(H = 100\ \text{Oe}) < R(H = 1\ \text{kOe})$. Such a surprising feature is explained below basing on the analysis of the hysteretic $R(H)$ dependences.

The temperature evolution of the $R(H)$ dependence is illustrated in Fig. 3. Figure 3a shows the $R(H)$ behavior at the weak transport current ($I = 1$ mA) in fields of up to 90 kOe at temperatures from 77 to 90 K. The $R(H)$ dependences measured at a significantly higher current of $I = 30$ mA in fields of up to 1 kOe in the same temperature range (77–90 K) are shown in Fig. 3b. In addition, Fig. 3b shows the hysteretic dependence of the magnetoresistance at a temperature of 4.2 K, which was obtained at a transport current of $I = 350$ mA. In Fig. 3, a double logarithmic scale is used due to the wide resistance and magnetic field ranges. The horizontal lines in Fig. 3 show the normal resistance R_{NJ} of the subsystem of grain boundaries. It can be seen in Fig. 3a that, in a sufficiently strong external field, the resistance of the sample attains this value. In the field H^* corresponding to $R \approx R_{NJ}$, the $R(H)$ dependences have a feature, specifically, the change in the curvature sign. This indicates the magnetoresistance saturation (plateau) in the subsystem of grain boundaries [38, 39]. With a further increase in the field, the resistance of the sample increases above the R_{NJ} value and, at $H \geq H^*$, the dissipation begins already in superconducting grains. The magnetoresistance hysteresis exists in fields from zero to H^*.

The hysteretic behavior of the magnetoresistance is qualitatively the same for the weak transport current (1 mA (Fig. 3a)) and for $I = 30$ mA and stronger (Fig. 3b): $R(H_{inc})$ is almost always greater than $R(H_{dec})$; hereinafter, H_{dec} and H_{inc} correspond to a decreasing and increasing external field. The $R(H_{inc})$ dependences in Fig. 3b are nonmonotonic and demonstrate the pronounced maximum and minimum with increasing field. It can be seen from the temperature evolution of the $R(H)$ dependences in Fig. 4b that, at $T = 77$ and 80 K, the inequality $R(H \approx 100\ \text{Oe}) > R(H \approx 1\ \text{kOe})$ is valid, whereas at $T = 82$ K, the resistances in these fields are approximately equal and, at temperatures above 82 K, $R(H_{inc} \approx 100\ \text{Oe})$ is already lower than $R(H_{inc} \approx 1\ \text{kOe})$. This is consistent with the atypical behavior of the $R(T)$ dependences measured at the same current $I = 30$ mA (see inset in Fig. 2).

Comparing the data presented in Figs. 3a and 3b for the temperature range of 77–90 K, we can state that, in a low transport current, the characteristic $R(H_{inc})$ local extrema are not observed. This is due to the fact that, at the sufficiently weak transport current, the dissipation begins in the fields stronger than the field in which the $R(H_{inc})$ anomalies arise. The $R(H)$ dependence at $T = 4.2$ K shown in Fig. 3b was obtained at the higher transport current ($I = 350$ mA) than the data for temperatures of 77–90 K in the figure. It can be seen that the $R(H_{inc})$ dependence at $T = 4.2$ K already does not contain characteristic local extrema, which, as we show below, is a nontrivial fact. Next, we consider in more detail the effect of the transport current on the magnetoresistance hysteresis type and the origin of the local $R(H_{inc})$ extrema.

Figure 4 shows the $R(H)$ dependences at different currents I and temperatures of 77 and 4.2 K in fields of up to 1 and 10 kOe, respectively (a double logarithmic scale is used). At $T = 77$ K, the magnetoresistance increases with the current and the shape of the $R(H)$ dependences somewhat changes. The maximum and minimum in the $R(H_{inc})$ dependence are observed at

all the transport currents used and their positions at different I values do not strongly differ. At $T = 4.2$ K, an increase in the current from 300 to 450 mA leads only to the occurrence of a noticeable magnetoresistance in weaker H_{inc} fields.

It was previously shown that, at sufficiently high temperatures (from 77 K to T_c), the hysteretic $R(H)$ dependences of granular HTSs exhibit a universal behavior: at T = const, the hysteresis field width is independent of the transport current [34, 35, 47, 50, 54]. This parameter is, in fact, the length of a segment connecting the points H_{dec} and H_{inc} in the hysteretic $R(H)$ dependence under the condition $R(H_{dec}) = R(H_{inc})$

$$\Delta H = H_{dec} - H_{inc}. \quad (3)$$

This behavior of the parameter ΔH follows directly from the implementation of a two-level superconducting system in a granular HTS, in which the transport current affects the dissipation in the subsystem of grain boundaries, but cannot affect the magnetization of grains and change the field B_{ind}. The horizontal lines connecting points in Fig. 4 correspond to the magnetoresistance hysteresis field width $\Delta H = H_{dec} - H_{inc}$ at $H_{dec} = 900$ Oe for the data at 77 K and $H_{dec} = 9800$ Oe for the data at 4.2 K. The points of intersection of the horizontal lines with the $R(H_{inc})$ dependence have the same abscissas (shown by vertical dashed lines). This illustrates the independence of the field hysteresis width of the transport current (at other H_{dec} values, ΔH is also independent of I). This property was previously described for the granular HTSs in the yttrium system, but at a temperature of 77 K [47, 50, 54]; in this study, the independence of ΔH on the transport current at $T = 4.2$ K is confirmed experimentally.

Let us consider the origin of local extrema in the $R(H_{inc})$ dependence. Figure 5 shows the hysteretic $M(H)$, $R(H)$, and $B_{eff}(H)$ dependences at $T = 80$ K. Equation (2) for the effective field in the intergrain medium contains unknown parameter α. This parameter can be determined basing on the following considerations. For any point in the $R(H_{dec})$ dependence, there is a point in the $R(H_{inc})$ dependence at which we have $R(H_{dec}) = R(H_{inc})$. Then, the effective field B_{eff} at the points with these abscissas (H_{dec} and H_{inc}) will be the same: $B_{eff}(H_{dec}) = B_{eff}(H_{inc})$. The $R(H)$ hysteresis width determined by Eq. (3) is independent of the transport current; therefore, it should have the same value as ΔH for the effective field: $\Delta H_{R = \text{const}} = \Delta H_{B_{eff}=\text{const}}$. Hence, at the α value that provides the best agreement between the ΔH values for the $R(H)$ hysteresis and the $B_{eff}(H)$ hysteresis, the obtained $B_{eff}(H)$ dependence will adequately reflect the effective field in the intergrain medium. The $B_{eff}(H)$ dependence shown in Fig. 5c was plotted at $\alpha = 20$ using the experimental magnetization data presented in Fig. 5a.

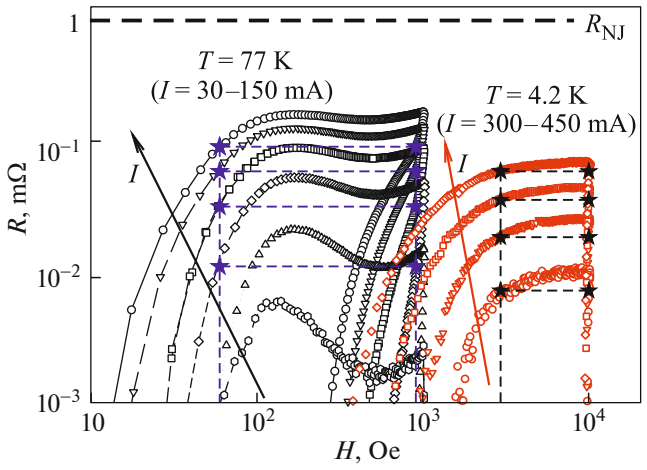

Fig. 4. $R(H)$ dependences at $T = 77$ K ($I = 30$, 50, 75, 100, 125, and 150 mA) and 4.2 K ($I = 300$, 350, 400, and 450 mA) in a double logarithmic scale. Horizontal and vertical dashed lines correspond to the same magnetoresistance hysteresis width at different I values.

It can be seen from Figs. 5b, 5c that the lengths of the horizontal segments (it is the hysteresis width ΔH) intersecting the $R(H)$ and $B_{eff}(H)$ dependences are almost identical. The segment lengths are consistent both when the horizontal straights R = const (B_{eff} = const) intersect the $R(H)$ and $B_{eff}(H)$ dependences four times and when the straights R = const only intersect them two times (the lower straights in Figs. 5b, 5c). In the $M(H)$ dependences (Fig. 5a), the points are also shown that meet to the conditions R = const and B_{eff} = const in Figs. 5b and 5c, respectively. Comparing the data in Figs. 5a, 5b, and 5c, we can unambiguously conclude that the local maximum in the $R(H_{inc})$ dependence corresponds to the extremum in the $M(H_{inc})$ dependence. As the temperature decreases from 88 to 77 K, the $R(H_{inc})$ maximum position shifts toward stronger fields (see Fig. 3b). This is caused by a shift in the extremum position in the $M(H_{inc})$ dependence with a decrease in temperature.

Let us consider in more detail the magnetoresistance at $T = 4.2$ K. The $R(H)$ dependence in the field range of ±60 kOe ($I = 350$ mA) is shown in Fig. 6b. This dependence has the form of a rectangular loop and drastically differs from the high-temperature data (see Figs. 3b, 5b). First, we estimate the parameter α characterizing the degree of magnetic flux compression in the intergrain medium. The horizontal dashed lines connecting the points in Fig. 6b have the same meaning as in Figs. 4 and 5b; in Fig. 6b, these lines correspond to the magnetoresistance hysteresis width ΔH at $H_{dec} = \pm 59.4$ kOe. The abscissa of the point of intersection of the horizontal lines in Fig. 6b and the $R(H_{inc})$ dependence is ±2.1 kOe; therefore, ΔH = 57.3 kOe. The magnetizations of the sample in fields of $H_{dec} = \pm 59.4$ kOe and $H_{inc} = \pm 2.1$ kOe can be seen

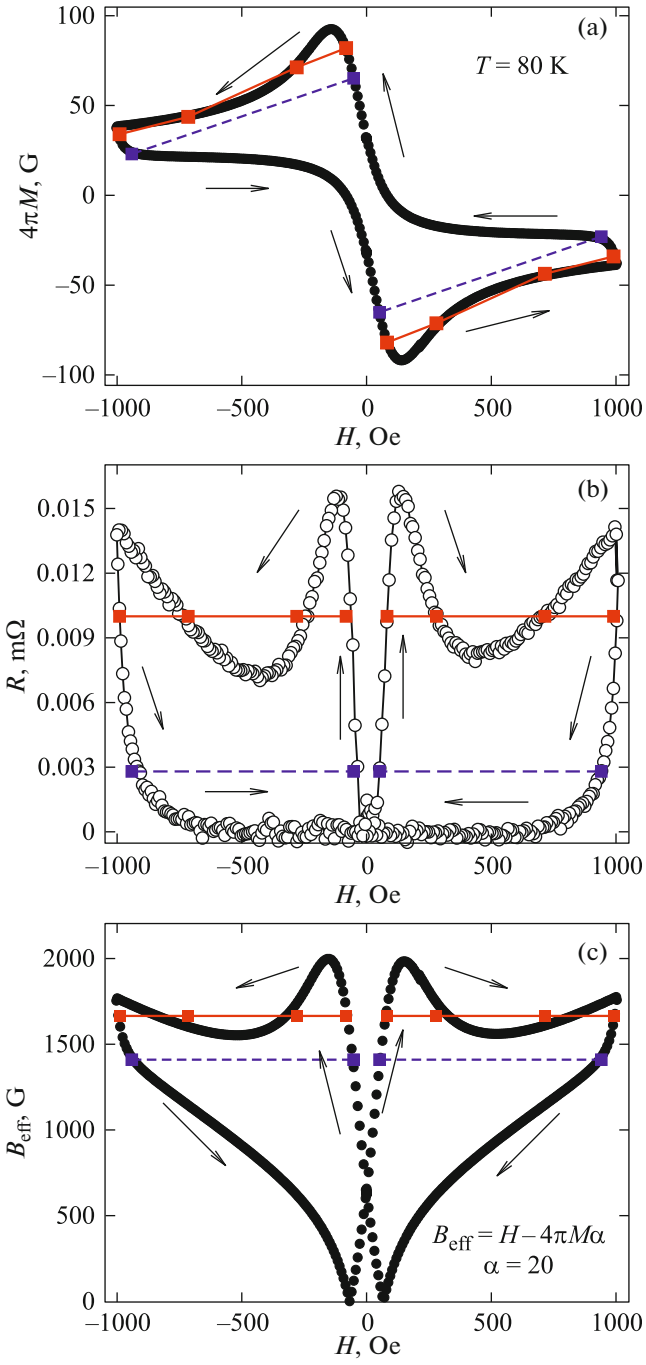

Fig. 5. Hysteretic (a) $M(H)$, (b) $R(H)$, and (c) $B_{\text{eff}}(H)$ dependences at $T = 80$ K. In (b, c), horizontal lines show that the ΔH values between the points in the $R(H)$ and $\mathbf{B}_{\text{eff}}(H)$ dependences are approximately the same. Arrows show the external field variation direction.

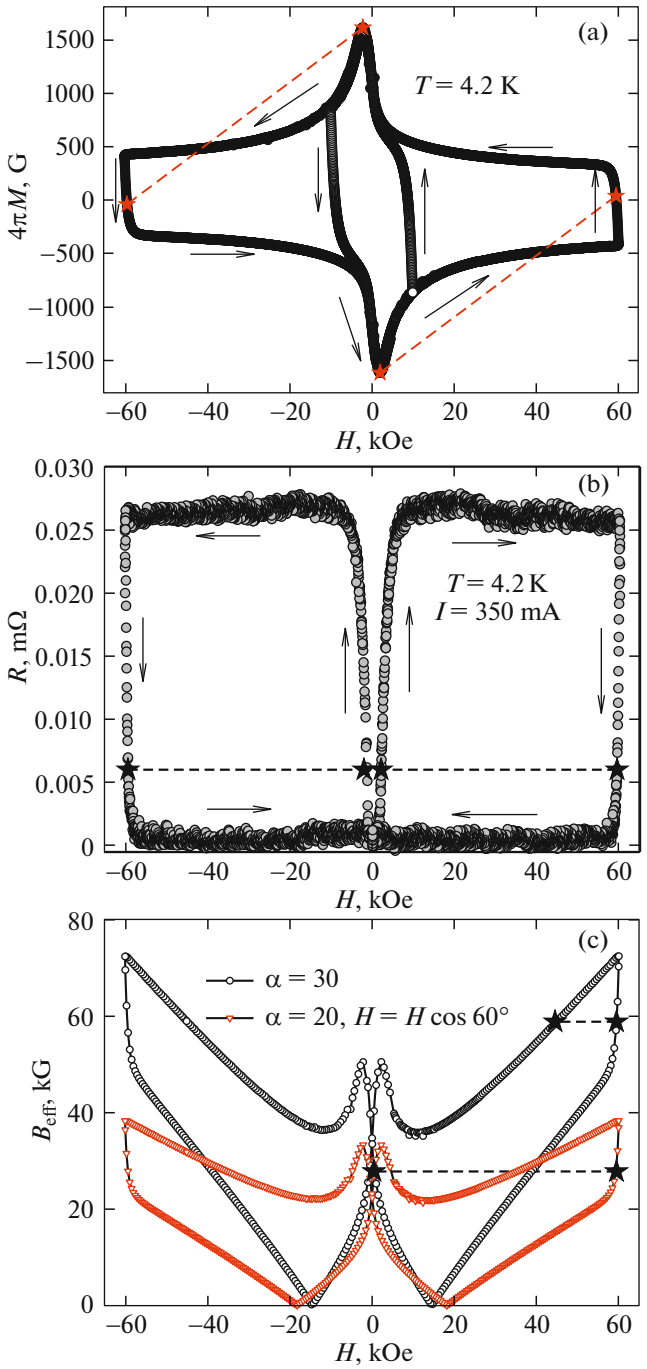

Fig. 6. Hysteretic (a) $M(H)$, (b) $R(H)$, and (c) $B_{\text{eff}}(H)$ dependences at $T = 4.2$ K. In (b, c), horizontal lines show that the $R(H)$ and $B_{\text{eff}}(H)$ hysteresis widths at $H_{\text{dec}} = 59.4$ kOe. In (c), the $B_{\text{eff}}(H)$ curves are built using Eq. (2) at the parameters shown in the figure.

in Fig. 6a. At $B_{\text{eff}}(H_{\text{dec}}) = B_{\text{eff}}(H_{\text{inc}})$, using Eqs. (2) and (3), we obtain

$$\Delta H = H_{\text{dec}} - H_{\text{inc}} = 4\pi\alpha\{M(H_{\text{dec}}) - M(H_{\text{inc}})\}. \quad (4)$$

Substituting the experimental magnetization values $M(H_{\text{dec}})$ and $M(H_{\text{inc}})$ and $\Delta H = 57.3$ kOe into Eq. (4), we find that the parameter α is about 30. Therefore, the degree of the magnetic flux compression did not

decrease at low temperature (at high temperatures, we have $\alpha \approx 20$), but rather increased.

However, the rectangular shape of the $R(H)$ dependence at 4.2 K in Fig. 6b is difficult to explain within the above-described approach. Indeed, the $B_{eff}(H)$ dependence in Fig. 6c built at $\alpha = 30$ using the magnetization data obtained at $T = 4.2$ K has both a local maximum and a local minimum, which are also observed at high temperatures. It should be noted that, at the large α values, the agreement between the $R(H)$ and $B_{eff}(H)$ hysteresis widths does not improve. If we decrease the α value when building the $B_{eff}(H)$ dependence, then the local $B_{eff}(H_{inc})$ maximum will be less pronounced; however, due to the dominance of the first term in Eq. (2), the ΔH value at $H_{dec} = \pm 59.4$ kOe will be much smaller than the ΔH value in the $R(H)$ dependence.

Thus, according to the comparative analysis of the experimental hysteretic $R(H)$ dependences at high temperatures and a low temperature (4.2 K), we can state that, at the low temperature, the model of hysteretic behavior of a granular HTS in an external field agrees with the experiment only qualitatively. The main incomprehensible fact is the absence of local extrema of the $R(H_{inc})$ dependence at $T = 4.2$ K (the rectangular shape). Let us discuss possible reasons for this behavior. Although the sample resistance at $T =$ 4.2 K, transport currents of $I =$ 300–450 mA, and fields of $H \sim$ 10–60 kOe is ~3–4% of the R_{NJ} value, it is nevertheless close to the resistance at temperatures of 77–80 K, transport currents of $I =$ 30–75 mA, and fields of $H \sim$ 0.1–1 kOe (see Figs. 3b and 4). Therefore, it cannot be assumed that the experimental conditions at $T = 4.2$ K are similar to the low-current conditions, as for the data in Fig. 3a, when the observed dissipation starts in strong fields. The $R(H)$ dependences at $T = 42$ K, as in the high-temperature region, do not demonstrate the transport current dependence of the field hysteresis width, which gives us grounds to use the parameter ΔH to analyze and compare by the hysteresis width of the effective field $B_{eff}(H)$. The degree of the flux compression in the intergrain medium determined by the α value at low temperatures remained at about the same level as in the high-temperature region ($\alpha \sim 20$–30).

Apparently, with a decrease in temperature, an additional factor arises that affects superconducting current carrier tunneling through grain boundaries. Such a factor may be the redistribution of microscopic current trajectories. According to the classical Bardeen–Stephen consideration [56], the magnetoresistance of a type-II superconductor is proportional to $\sin^2(\angle \mathbf{H}, \mathbf{I})$; i.e., at $\mathbf{H} \perp \mathbf{I}$ (which corresponds to the experimental conditions), the destruction of Cooper pairs is most effective and the magnetoresistance is maximum [48, 49, 57–61]. For microscopic currents $\mathbf{I}_m$ (Fig. 1b), we have $R \sim \sin^2(\angle \mathbf{H}, \mathbf{I}_m)$. With a decrease in temperature (for example, from 80 to 4.2 K (Figs. 5a and 6a), the magnetization value, which determines the induced field B_{ind}, increases by more than an order of magnitude. Possibly, with a strong increase in the effective field, it will be preferable for carriers to tunnel through the neighboring grain, if the angle between $\mathbf{B}_{ind}$ and $\mathbf{I}_m$ is small. In fact, the microscopic current trajectories can flow around the grain boundaries, in which $\mathbf{B}_{eff} \perp \mathbf{I}$. Such a redistribution of the microscopic current trajectories is schematically shown in Fig. 1c (compare with Fig. 1b). In this case, tunneling will occur through intergrain spacings, in which $\angle \mathbf{B}_{eff}, \mathbf{I}_m < 90°$ and, therefore, $\angle \mathbf{H}, \mathbf{I}_m$ is smaller than 90°. Then, the effect of the external field will be weaker and the projection of $\mathbf{H}$ onto the Z plane perpendicular to the microscopic current trajectory will work (Fig. 1c). The value of this projection can be written as $H\cos\beta$, where $\beta = \angle \mathbf{I}, \mathbf{I}_m$ (Fig. 1c). Figure 6c shows the $B_{eff}(H)$ dependence at $\alpha = 20$; the external field in Eq. (2) was taken with a coefficient of 0.5, i.e., $\beta = 60°$. Certainly, it cannot be said that this $B_{eff}(H)$ dependence describes well the magnetoresistance behavior (Fig. 6b). Nevertheless, the values $B_{eff}(H \approx$ 60 kOe) and $B_{eff}(H_{inc} \approx$ 1.5 kOe) (the field $H_{inc} \approx$ 1.5 kOe corresponds to the $B_{eff}(H_{inc})$ local maximum) are already close (in contrast to these quantities for the $B_{eff}(H)$ dependence at $\alpha = 30$). If we take into account that during the redistribution of current trajectories, the parameter α can depend on the external field (this is fairly difficult to take into account in simple equation (2)), then we can say that, at the replacement $H \rightarrow H\cos\beta$, the $B_{eff}(H)$ dependence explains better, although qualitatively, the magnetoresistance hysteresis at $T = 4.2$ K. Note that the obtained β value means that the microscopic currents can deviate from the macroscopic current direction by up to ~60°, which is quite expected in this scenario.

4. CONCLUSIONS

To sum up, the hysteretic field dependences of the magnetoresistance for a granular $YBa_2Cu_3O_{7-\delta}$ HTS sample with the fairly high transport characteristics ($J_c(T = 77$ K) $\approx$ 150 A/cm^2, $J_c(T = 4.2$ K) $\approx$ 1.5 kA/cm^2 at $H = 0$) at different transport current densities were studied in the temperature range from 77 K to the transition temperature T_c and at $T = 4.2$ K. The measurements covered wide transport current and magnetic field (up to 90 kOe) ranges. The results obtained were analyzed using the developed model of the behavior of a granular HTS in an external magnetic field, in which the magnetoresistance is a function of the effective field in the intergrain medium: $B_{eff}(H) = |H - 4\pi\alpha M(H)|$.

At high temperatures (from 77 K to T_c), all the features in the $R(H)$ dependence are adequately described by the model. These are (i) the indepen-

dence of the $R(H)$ hysteresis field width ΔH of the transport current, (ii) a fairly large ΔH value, which characterizes the strong magnetic flux compression in the intergrain medium, and (iii) the pronounced local maximum in the $R(H)$ dependence with increasing external field. The first two features are observed also for the data obtained at 4.2 K; however, the local maximum pronounced in the high-temperature region is not observed in the $R(H)$ dependence. This is indicative of the occurrence of an additional factor affecting the dissipation in the intergrain medium at low temperatures. This factor can be the redistribution of the microscopic current trajectories, which occurs upon the external magnetic field variation. In other words, at low temperatures, under the strong flux compression, the microscopic current trajectories can change, when tunneling occurs preferably through the intergrain boundaries in which the microcurrent direction is not perpendicular to the effective field strength lines (at $\mathbf{H} \perp \mathbf{I}$). The investigated sample has the characteristics typical of granular HTS materials of the yttrium system, which gives us grounds to generalize our conclusions to, at least, the class of granular materials of this HTS system.

ACKNOWLEDGMENTS

The authors are grateful to D.M. Gokhfeld for discussion of the results. The measurements of the transport properties were performed in part on a PPMS-6000 facility at the Krasnoyarsk Territorial Center of Collective Use, Krasnoyarsk Scientific Center, Siberian Branch, Russian Academy of Sciences.

CONFLICT OF INTEREST

The authors declare that they have no conflicts of interest.

REFERENCES

1. J. Jung, M. A.-K. Mohamed, S. C. Cheng, and J. P. Franck, Phys. Rev. B **42**, 6181 (1990).
2. B. Andrzejewski, E. Guilmeau, and Ch. Simon, Supercond. Sci. Technol. **14**, 904 (2001).
3. E. B. Sonin, JETP Lett. **47**, 496 (1988).
4. D.-X. Chen, R. W. Cross, and A. Sanchez, Cryogenics **33**, 695 (1993).
5. V. V. Val'kov and B. P. Khrustalev, J. Exp. Theor. Phys. **80**, 680 (1995).
6. D. M. Gokhfeld, Phys. Solid State **56**, 2380 (2014).
7. M. A. Dubson, S. T. Herbet, J. J. Calabrese, D. C. Harris, B. R. Patton, and J. C. Garland, Phys. Rev. Lett. **60**, 1061 (1988).
8. M. I. Petrov, S. N. Krivomazov, B. P. Khrustalev, and K. S. Aleksandrov, Solid State Commun. **82**, 453 (1992).
9. M. I. Petrov, D. A. Balaev, B. P. Khrustalev, and K. S. Aleksandrov, Phys. C (Amsterdam, Neth.) **235–240**, 3043 (1994).
10. J. E. Evetts and B. A. Glowacki, Cryogenics **28**, 641 (1988).
11. E. Altshuler, J. Musa, J. Barroso, A. R. R. Papa, and V. Venegas, Cryogenics **33**, 308 (1993).
12. P. Mune, E. Govea-Alcaide, and R. F. Jardim, Phys. C (Amsterdam, Neth.) **354**, 275 (2001).
13. P. Mune, F. C. Fonseca, R. Muccillo, and R. F. Jardim, Phys. C (Amsterdam, Neth.) **390**, 363 (2003).
14. D. A. Balaev, D. M. Gokhfeld, S. I. Popkov, K. A. Shaykhutdinov, and M. I. Petrov, Phys. C (Amsterdam, Neth.) **460–462**, 1307 (2007).
15. D. A. Balaev, A. A. Dubrovskii, S. I. Popkov, D. M. Gokhfeld, S. V. Semenov, K. A. Shaykhutdinov, and M. I. Petrov, Phys. Solid State **54**, 2155 (2012).
16. C. A. M. dos Santos, M. S. da Luz, B. Ferreira, and A. J. S. Machado, Phys. C (Amsterdam, Neth.) **391**, 345 (2003).
17. S. Shifang, Z. Yong, P. Guoqian, Y. Daoq, Z. An, C. Zuyao, Q. Yitai, K. Eiyan, and Z. Qirui, Europhys. Lett. **6**, 359 (1988).
18. L. Ji, M. S. Rzchowski, N. Anand, and M. Tinkham, Phys. Rev B **47**, 470 (1993).
19. M. Prester, E. Babic, M. Stubicar, and P. Nozar', Phys. Rev. B **49**, 6967 (1994).
20. M. Prester, Supercond. Sci. Technol. **11**, 333 (1998).
21. D. Daghero, P. Mazzetti, A. Stepanescu, and P. Tura, Phys. Rev. B **66**, 11478 (2002).
22. N. D. Kuz'michev, JETP Lett. **74**, 262 (2001).
23. N. D. Kuz'michev, Phys. Solid State **43**, 2012 (2001).
24. A. A. Sukhanov and V. I. Omelchenko, J. Low Temp. Phys. **29**, 297 (2003).
25. V. V. Derevyanko, T. V. Sukhareva, and V. A. Finkel', Phys. Solid State **46**, 1798 (2004).
26. V. V. Derevyanko, T. V. Sukhareva, and V. A. Finkel', Phys. Solid State **49**, 1455 (2007).
27. T. V. Sukhareva and V. A. Finkel, Phys. Solid State **50**, 1001 (2008).
28. V. V. Derevyanko, T. V. Sukhareva, and V. A. Finkel, Tech. Phys. **53**, 321 (2008).
29. T. V. Sukhareva and V. A. Finkel, Phys. Solid State **53**, 914 (2011).
30. V. V. Derevyanko, T. V. Sukhareva, V. A. Finkel, and Yu. N. Shakhov, Phys. Solid State **56**, 649 (2014).
31. V. V. Derevyanko, T. V. Sukhareva, and V. A. Finkel', Phys. Solid State **59**, 1492 (2017).
32. V. V. Derevyanko, T. V. Sukhareva, and V. A. Finkel', Phys. Solid State **60**, 470 (2018).
33. M. A. Vasyutin, Tech. Phys. Lett. **39**, 1078 (2013).
34. D. A. Balaev, D. M. Gokhfeld, A. A. Dubrovski, S. I. Popkov, K. A. Shaikhutdinov, and M. I. Petrov, J. Exp. Theor. Phys. **105**, 1174 (2007).
35. D. A. Balaev, A. A. Dubrovskii, K. A. Shaikhutdinov, S. I. Popkov, D. M. Gokhfeld, Yu. S. Gokhfeld, and M. I. Petrov, J. Exp. Theor. Phys. **108**, 241 (2009).
36. D. A. Balaev, A. A. Dubrovskii, S. I. Popkov, K. A. Shaikhutdinov, and M. I. Petrov, Phys. Solid State **50**, 1014 (2008).
37. K. A. Shaikhutdinov, D. A. Balaev, S. I. Popkov, and M. I. Petrov, Phys. Solid State **51**, 1105 (2009).

38. D. A. Balaev, A. A. Bykov, S. V. Semenov, S. I. Popkov, A. A. Dubrovskii, K. A. Shaikhutdinov, and M. I. Petrov, Phys. Solid State **53**, 922 (2011).
39. D. A. Balaev, S. I. Popkov, S. V. Semenov, A. A. Bykov, E. I. Sabitova, A. A. Dubrovskiy, K. A. Shaikhutdinov, and M. I. Petrov, J. Supercond. Nov. Magn. **24**, 2129 (2011).
40. D. A. Balaev, S. I. Popkov, K. A. Shaikhutdinov, M. I. Petrov, and D. M. Gokhfeld, Phys. Solid State **56**, 1542 (2014).
41. D. M. Gokhfeld, D. A. Balaev, S. V. Semenov, and M. I. Petrov, Phys. Solid State **57**, 2145 (2015).
42. M. Olutas, A. Kilic, K. Kilic, and A. Altinkok, J. Supercond. Nov. Magn. **26**, 3369 (2013).
43. A. Altinkok, K. Kilic, M. Olutas, and A. Kilic, J. Supercond. Nov. Magn. **26**, 3085 (2013).
44. M. Olutas, A. Kilic, K. Kilic, and A. Altinkok, Eur. Phys. J. B **85**, 382 (2012).
45. D. A. Balaev, S. I. Popkov, E. I. Sabitova, S. V. Semenov, K. A. Shaykhutdinov, A. V. Shabanov, and M. I. Petrov, J. Appl. Phys. **110**, 093918 (2011).
46. D. A. Balaev, S. V. Semenov, and M. I. Petrov, J. Supercond. Nov. Magn. **27**, 1425 (2014).
47. D. A. Balaev, S. V. Semenov, and M. I. Petrov, Phys. Solid State **55**, 2422 (2013).
48. S. V. Semenov, D. A. Balaev, M. A. Pochekutov, and D. A. Velikanov, Phys. Solid State **59**, 1291 (2017).
49. D. A. Balaev, S. V. Semenov, and M. A. Pochekutov, J. Appl. Phys. **122**, 123902 (2017).
50. S. V. Semenov and D. A. Balaev, Phys. C (Amsterdam, Neth.) **550**, 19 (2018).
51. S. V. Semenov and D. A. Balaev, J. Supercond. Nov. Magn. **32**, 2409 (2019).
52. S. V. Semenov, A. D. Balaev, and D. A. Balaev, J. Appl. Phys. **125**, 033903 (2019).
53. A. D. Balaev, Yu. V. Boyarshinov, M. M. Karpenko, and B. P. Khrustalev, Prib. Tekh. Eksp., No. 3, 167 (1985).
54. D. A. Balaev, A. A. Dubrovskii, S. I. Popkov, D. M. Gokhfeld, S. V. Semenov, K. A. Shaikhutdinov, and M. I. Petrov, Phys. Solid State **54**, 2155 (2012).
55. M. A. Vasyutin, N. D. Kuz'michev, and D. A. Shilkin, Phys. Solid State **58**, 236 (2016).
56. J. Barden and M. J. Stephen, Phys. Rev. A **140**, 1197 (1965).
57. D. Lopez and F. de la Cruz, Phys. Rev. B **43**, 11478 (1991).
58. D. Lopez, R. Decca, and F. de la Cruz, Supercond. Sci. Technol. **5**, 276 (1992).
59. O. V. Gerashchenko and S. L. Ginzburg, Supercond. Sci. Technol. **13**, 332 (2000).
60. D. A. Balaev, A. G. Prus, K. A. Shaukhutdinov, D. M. Gokhfeld, and M. I. Petrov, Supercond. Sci. Technol. **20**, 495 (2007).
61. A. Kilic, K. Kilic, S. Senoussi, and K. Demir, Phys. C (Amsterdam, Neth.) **294**, 203 (1998).

Translated by E. Bondareva